\$ S LINE ELSEVIER

Contents lists available at ScienceDirect

Materials Today Physics

journal homepage: www.journals.elsevier.com/materials-today-physics





MoO_{3-x} quantum dots-based hydrogel with excellent light-triggered self-healing efficiency and pressure sensitive photoluminescence for accurate remote force measurement

Yiqiang Li ^{a,1}, Yuanyuan Mi ^{a,1}, Zheyu Liu ^a, Yinping Liu ^a, Weiye Zhang ^a, Shangxing Qiu ^a, Melvin A. Ramos ^b, Travis Shihao Hu ^b, Quan Xu ^{a,*}

ARTICLE INFO

Keywords: Composite hydrogel MoO_{3-x} quantum dots Self-healing Photoluminescence Remote measurement

ABSTRACT

Multi-responsive functional materials with simultaneous photothermal and photoluminescent properties have broad applicational prospects in the field of flexible electronics, devices and remote force detection and monitor. Here, a feasible method is developed by introducing MoO_{3-x} quantum dots $(MoO_{3-x}$ QDs) and blue fluorescent carbon dots (B-CDs) into a strong hydrogel matrix to fabricate a novel composite hydrogel with concurrent photothermal and photoluminescent properties. Besides rendering the peculiar multifunctionalities, we found that the addition of photothermal MoO_{3-x} QDs enhances the mechanical properties and self-healing properties of the composite hydrogel. The temperature of the MoO_{3-x} -CDs-PVA (Polyvinyl Alcohol) hydrogel can rise by 30 °C within 1 min after 808 nm infrared laser irradiation and the self-healing efficiency could double after 40 s of irradiation. Moreover, there is a good linear relationship between the fluorescence intensity of the composite hydrogel and the external force, which can be used to monitor the force within a certain range. The monitoring range and sensitivity can be further improved by adjusting the infrared laser to for small force detection. Finally, the novel composite hydrogel is successfully applied to fracture monitoring in fracturing and force monitoring at different locations in the fluid model in the field of petroleum engineering.

1. Introduction

Self-healing hydrogel is a type of novel material, which can self-repair from mechanical damage by reconstructing the three-dimensional network structure through dynamic covalent [1–4] and/or non-covalent cross-linking [5–8]. This material attribute is very attractive, where excellent stretchability, high strength and long fatigue life is of a big concern. In particular, self-healing hydrogels with multi-functional stimuli-responsiveness, such as electrical [9–11], magnetic [12–14], optical [15], and thermal [16], have attracted a great amount of attention in recent years. These functional materials are able to respond to external stimuli by actively adjusting their properties, while maintaining the characteristics of high levels of flexibility and conformability. The synergy among the multiple functionalities has broad application prospects in the fields of flexible electronics, devices

and sensors [17], critically needed in the biomedical [18], engineering [19–21] and energy related fields.

The hydrogels doped with quantum dots in order to achieve modified and improved functionalities and mechanical performances have been widely reported. Molybdenum-based nanomaterials have been incorporated into hydrogels because of their good photothermal conversion properties, which enable the composite materials to efficiently absorb infrared light and converted it into heat. Recently, Li et al. proposed a strategy of doping plasmonic H_xMoO_3 quantum dots into PNIPAm (poly (N-isopropylacrylamide)) hydrogels to obtain multifunctionalities [22]. The addition of quantum dots into the polymeric system enhances the photothermal conversion, mechanical properties, adhesion, and self-healing performance simultaneously. The $H_xMoO_3/PNIPAm$ hydrogel has good macrophage (MØ) growth promoting activity on wounds. Xu et al. fabricated a molybdenum disulfide (MoS₂)

^a State Key Laboratory of Petroleum Resources and Prospecting, Beijing Key Laboratory of Biogas Upgrading Utilization, China University of Petroleum, Beijing, 102249, China

^b Department of Mechanical Engineering, California State University, Los Angeles, CA, 90032, United States

^{*} Corresponding author.

E-mail address: xuquan@cup.edu.cn (Q. Xu).

¹ Those authors contribute equally to this work.

nanosheets-based hydrogel (Gel-PEG-MoS₂, GPM hydrogel), with near-infrared (NIR) light-induced self-healing property, which is applied to a flexible sensor [23]. In previous work, we have reported a fluorescence-responsive self-healing hydrogel, which showed a good response to the forces exerted on the hydrogel. The forces and the self-healing efficiency could be determined by measuring the intensity of the excitation peak [24]. However, the hydrogel has a limited detection range (>0.98 N), which limits its application.

In present work, we choose to dope MoO3-x QDs with photoluminescent hydrogels. Under 808 nm infrared light irradiation, the selfhealing efficiency is improved by 70% compared with the unexposed hydrogel, owing to the photothermal effect. The flexibility of the polymer chain is increased due to the high-efficiency photothermal conversion performance of the composite hydrogels. The hydrogen bonds between the molecular chains disappear after infrared light irradiation, and the hydrogel becomes more sensitive to external force and easier to deform. Under normal conditions, the force detection range of the fluorescent hydrogel is restrained. After near-infrared illumination, the hydrogel is more sensitive to the detection of small forces (<0.98 N), thus increasing the force monitoring range. The mechanism of the photo-induced phenomenon is different from the piezoresistive effect [25,26] and the piezoelectric effect [27] in force monitoring and detection. The proposed mechanism is based on the change of fluorescent intensity and the consequential change in the material's mechanical response to external loadings or forces. This MoO_{3-x}-CDs-PVA hydrogel is successfully demonstrated to be applicable in fracture monitoring in artificial fracturing, and in monitoring a planar radial flow pressure field.

2. Experimental

2.1. Materials

PVA (degree of polymerization: 2699) was purchased from Anhui Wanwei Group Co. Agarose (Analytical Grade) was purchased from Life Technologies Corporation. Glycerol was purchased from Beijing Solarbio Science Technology Co. Ltd (Analytical Grade). Chitosan was purchased from Beijing Bellingway Technology Co. Ltd. Sodium tetraborate (Analytical Grade: Na₂B₄O₇·10H₂O) and Manganese carbonate were purchased from Tianjin Guangfu Technology Development Co. Ltd. Hydrogen peroxide was purchased from Beijing Chemical Reagent. Molybdenum powder was purchased from Chengdu XiYa Chemical Co., Ltd. The Sodium citrate and Citric acid monohydrate were purchased from Alladin. The core adopts a natural tight sandstone core, the specifications of which are gas permeability 0.3 mD, porosity 12.8%, diameter 2.5 cm, and length 7.5 cm. The slab model uses an artificial core cemented with epoxy resin to simulate a 1/4 five-point well pattern. The model size is $30 \times 30 \times 4.5 \text{ cm}^3$, with an average gas permeability of 89 mD and a porosity of 19.2%. There are 8 wells on the model. Among them, 5 pressure wells (injection wells can measure pressure).

2.2. Preparation of MoO_{3-x} quantum dots

Firstly, 0.5 g molybdenum powder was added into the 7.5 mL of hydrogen peroxide solution (30%) and reacted to light yellow homogeneous solution in ice water bath. The resulting solution was diluted into a 30 ml solution with deionized water. Next, the solution was sonicated for 2 h to remove the unreacted hydrogen peroxide. After that, 1 g of chitosan was added to the resulting solution and stirred for 10 min. The solution was then transferred to a Teflon lined autoclave and then underwent hydrothermal reaction in an electric oven at 80 $^{\circ}\text{C}$ for 8 h. The product was obtained via dialysis for 3 days.

2.3. Preparation of B-CDs

The hydrothermal method was employed to prepare the blue carbon dots. 0.735 g sodium citrate, 0.2 g citric acid monohydrate and 2 g $MnCO_3$ were added into 25 ml deionized water and stirred evenly. The solution was placed into a 50 ml Teflon-lined stainless-steel autoclave, which was kept in a furnace at 195 $^{\circ}C$ for 2 h.

2.4. Preparation of the CDs-MoO_{3-x}-PVA hydrogel

Firstly, PVA (10 g), agarose (0.5 g), chitosan (0.5 g) and glycerin (2 mL) were dissolved in deionized water to form a 50 mL solution and magnetically stirred. Next, different proportions of MoO $_{\rm 3-x}$ QDs and 2 ml B-CDs were added to the solution, which was oil-bathed at 98 °C for 2 h. After that, 50 ml of a borax solution (0.04 mol/L) was mixed with the heated mixture and oil-bathed at 80 °C for 1 h. Finally, the resulting hydrogel was kept in a petri dish at 4 °C in the humidity chamber for 3 days.

2.5. Characterization

Zeiss Sigma 500 and Bruker XFlash 6/30 were used to capture the scanning electron microscope (SEM) and energy-dispersive X-ray spectroscopy (EDX) imaging on the freeze-dried hydrogel samples. Fourier transform infrared spectroscopy (FTIR) was conducted using Nicolet IS10 infrared spectrometer to study the bond information and functional groups. The photothermal effect of the samples was recorded with an Infrared Thermal Imager (Testo 865) under the NIR laser light (808 nm). The composite hydrogel was irradiated for 10 min. The temperature was monitored and recorded by an infrared thermal imager one time per $30\,\mathrm{s}$ simultaneously. Fluorescence experiments were performed using UV lamps (12 W-ZF-7A-254-365 nm) and purple LED chips (3 W-Violet-400-405 nm). The fluorescence intensity of the hydrogel was measured with a Fluorescence Spectrometer (FS5, Edinburgh). The optical properties were measured using a UV-Vis-NIR spectrophotometer (UH4150, HITACHI, Japan). Transmission electron microscopy (TEM) images were obtained using a microscope at an acceleration voltage of 300 kV (FEI Tecnai G2 F30).

2.6. Mechanical properties and characterization

The hydrogel was prepared in a negative dumbbell shaped mold (gage length: $6\times 16\times 36~\text{mm}^3$) for tensile testing and self-healing tests. All measurements were taken with Instron universal testing machine (INSTRON 5567). A fixed rate of extension (50 mm/min) was applied to all tensile testing. The measured engineering stresses and nominal stresses were calculated by the following formula: $\sigma=\frac{F}{4}$

In this formula, F is the applied load on the composite hydrogel; A_0 is the initial cross-sectional area. The hydrogel was cut into two pieces of equal size. In order to prevent the healing time error caused by the operation during the test, two pieces of hydrogel were placed on both ends of the stretching machine in advance, and they were stretched after being connected again for a different time (10 s, 20 s, 30 s, 40 s, 50 s, 60 s).

2.7. Monitoring the fracturing fractures using the hydrogel

The different positions of the core are divided into areas, and hydrogels of uniform size (0.8 cm \times 0.8 cm) are pasted on the divided areas (1.5 cm \times 1.5 cm \times 9). In order to prevent the position of the hydrogel from moving during fracturing, tape was used to fix the hydrogel at each position. Then, the core with the hydrogel is uniaxially fractured using a Hassler-type core holder. After fracturing the core, the hydrogel on the fractured core is removed to test its fluorescence intensity. Combining the fluorescence intensity of the hydrogel at the

divided points of different regions, the surfer software is used to draw a field diag to simulate the crack shape (Fig. S8).

2.8. Monitoring the flow field pressure using the hydrogel

First, put the uncured composite hydrogel into the hole of the pressure testing valve, and wait for it to solidify and shape up. Secondly, use gas cylinders to respectively pressurize to 0, 0.05 MPa, 0.1 MPa, 0.2 MPa, and 0.3 MPa, and the hydrogel was taken out after stabilization to measure fluorescence intensity using the spectrometer. Then, fix the valve loaded with the composite hydrogel on the pressure measuring point of the plane model, and inject gas from the injection well of the plane model with a gas cylinder. After waiting for a period of time to stabilize, take out the hydrogel from the pressure measuring points and measure the fluorescence intensity. Finally, combined with the standard curve to determine the corresponding pressure, use surfer software to draw the pressure field distribution map (Fig. S9).

3. Results and discussion

3.1. Design principle and synthesis of MoO_{3-x}-CDs-PVA hydrogel

PVA, B-CDs and MoO_{3-x} QDs were employed to fabricate the hydrogels with photothermal and fluorescent properties by a one-pot sol-gel synthesis method. The typical preparation strategy was composed of three steps, which include the hydrothermal preparation of MoO_{3-x} QDs and metal-doped CDs, and the preparation of light-responsive fluorescent hydrogels. As shown in Fig. 1a, MoO_{3-x} QDs were fabricated via a hydrothermal method in which metallic Mo was used as the Mo source and chitosan functioned as both the capping agent and reducing agent at 80 °C for 8 h [28]. The morphology of MoO_{3-x} QDs

was characterized by TEM (Fig. S1), showing the MoO_{3,v} QDs with uniform distribution of size between 2.5 and 3.9 nm. Blue carbon dots are prepared by hydrothermal method using sodium citrate and MnCO₃ as precursors (Fig. 1b). Citric acid is used to acidify the solution to increase the solubility of manganese carbonate. The TEM image shows that B-CDs have a spherical structure with a diameter distribution between 2.2 and 3.8 nm (Fig. S2) without agglomeration. Subsequently, adding MoO_{3-x} QDs and the B-CDs into the hydrogel provides the hydrogels with photoluminescence and photothermal properties. Due to its high mechanical strength and elasticity, PVA was selected as the primary polymer network structure for the composite hydrogel. The PVA, agarose, and chitosan are physically cross-linked with each other to form the backbone network of the hydrogel, so that the hydrogel maintains a specific shape and stable mechanical properties. The self-healing properties of the as-prepared hydrogel are attributed to the reversible network consisting of two dynamic covalent cross-linking reactions of PVA-borax-PVA [29] and PVA-glycerol-PVA [30]. The MoO_{3-x} QDs and the B-CDs were uniformly dispersed in the hydrogel to ensure robust photoluminescence and photothermal response (Fig. 1c).

3.2. Photothermal property of MoO_{3-x}-CDs-PVA hydrogel

The molecular structure of the MoO_{3-x} -CDs-PVA hydrogel is shown in Fig. 2a. Due to the use of chitosan as the capping agent, the MoO_{3-x} QDs could interact with the functional groups on the polymer chain of the hydrogel through hydrogen bonding. Fig. 2b shows the Fourier transform infrared spectroscopy (FTIR) spectra of PVA, CDs-PVA, and MoO_{3-x} -CDs-PVA hydrogel. In the FTIR spectra, the peak positions of the hydroxyl groups of PVA and CDs-PVA are not significantly shifted. However, the –OH stretching band in the MoO_{3-x} -CDs-PVA is located at 3262 cm $^{-1}$, which shifts to a lower wavenumber compared with that of

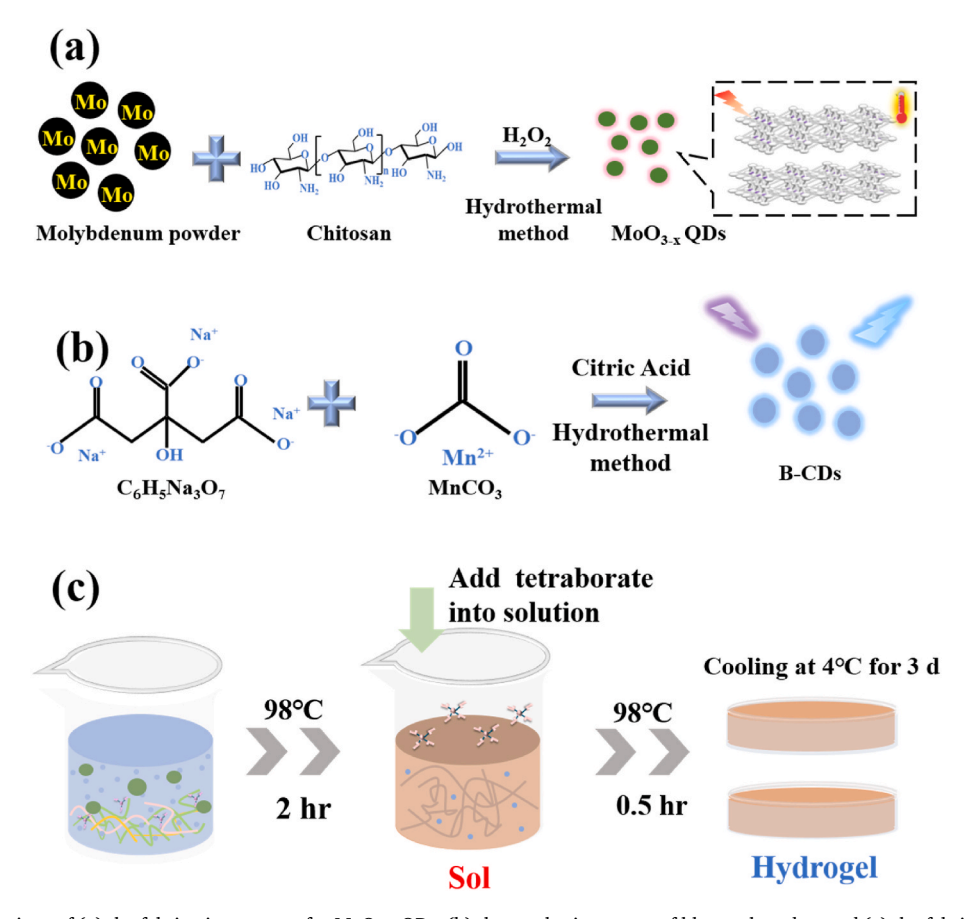


Fig. 1. Schematic illustrations of (a) the fabrication process for MoO_{3-x} QDs, (b) the synthesis process of blue carbon dots and (c) the fabrication process of MoO_{3-x} CDs-PVA hydrogel. (For interpretation of the references to colour in this figure legend, the reader is referred to the Web version of this article.)

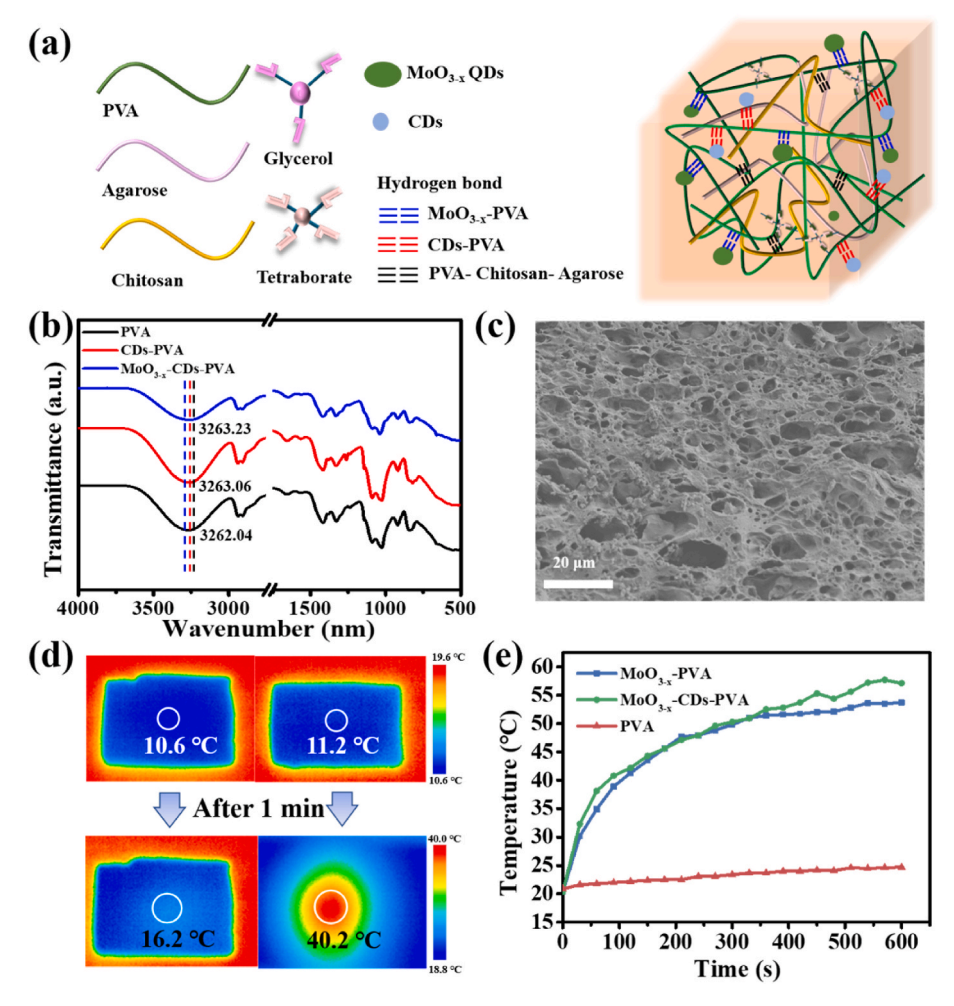


Fig. 2. (a) Schematic of the internal structure of the MoO_{3-x} -CDs-PVA hydrogel. (b) FTIR spectra of the different hydrogels (c) SEM images of MoO_{3-x} -CDs-PVA hydrogel. (d)NIR images revealing temperature variations of pure hydrogel and composite hydrogel in 1 min, MoO_{3-x} content: 1 g (weight ratio: 1%). (e) The time-temperature response curves of different hydrogel samples (MoO_{3-x} -PVA, MoO_{3-x} -CDs-PVA, and pure PVA) in a unit reaction system under 808 nm NIR laser.

pristine PVA and CDs-PVA (3263 cm⁻¹), indicating that hydrogen bonding is formed between the hydroxyl groups of PVA and the functional groups of MoO3-x QDs. The porous morphology of freeze-dried hydrogels was characterized by a scanning electron microscope (SEM). Compared to a hydrogel without MoO_{3-x} QDs (Fig. S3), the MoO_{3-x}-CDs-PVA hydrogel assumes a more compact porous structure, suggesting that the synthesized hydrogel possesses a higher crosslinking density (Fig. 2c). As shown in the energy-dispersive X-ray spectroscopy (EDX) results of the synthesized hydrogel, molybdenum and manganese elements can be observed on the surface, indicating the MoO_{3-x} QDs and the B-CDs were homogeneously dispersed in the hydrogels (Fig. S4). The photothermal properties of the composite hydrogel are expected to be originated from the doped MoO_{3-x} QDs. Hence, we evaluated the photothermal conversion properties by measuring the thermal variations of the MoO_{3-x} dots aqueous suspensions under 880 nm NIR laser irradiation in real-time via an infrared thermal camera. As shown in Fig. S5, the control (i.e., deionized water) shows a negligible temperature rise upon laser irradiation. In sharp contrast, all of the MoO_{3-x} QDs dispersions exhibited remarkable temperature elevation over time. Subsequently, photothermal stability tests of different hydrogels were carried out. The temperature of the MoO_{3-x}-CDs-PVA hydrogel reaches 40.2 °C in 1 min at the optimal mixing ratio (1% MoO_{3-x}), while the pure hydrogel kept a relatively low temperature of 16.2 °C (Fig. 2d). The temperatures of hydrogel samples with different contents of MoO_{3-x} QDs were recorded every 30 s, and the experimental results are shown in Fig. 2e. Compared with the hydrogel without MoO_{3-x} QDs, the temperature of MoO_{3-x}

doped hydrogel could rise to 50 $^{\circ}$ C in 5 min from an initial temperature of 20 $^{\circ}$ C. This result indicates the MoO_{3-x} QDs still preserve the excellent light-to-heat conversion effect in the hydrogel. By comparison, doping of blue fluorescent carbon dots has minimal effect on the photothermal conversion properties of the hydrogel.

3.3. Mechanical performance of MoO_{3-x}-CDs-PVA hydrogel

Next, the mechanical performance of the composite hydrogel where the PVA content was fixed at 20% (m/v), and the solid contents of MoO₃. x QDs were set at 1%, 2%, and 3% (m/v), were experimented and discussed. As shown in Fig. 3a, the stretchability of the PVA-MoO_{3-x} (2%) hydrogel reached 480% strain with a tensile strength of 86 KPa, with the best mechanical performance among the three samples. This suggests that moderate number of MoO_{3-x} QDs could improve the overall strength of the gel material as reinforcements, while excessive MoO3-x QDs incorporated into the hydrogel would negatively affect the polymerization of the hydrogel and cause its mechanical strength to decrease. As the content of doped MoO_{3-x} QDs was increased from 2% to 3%, the fracture stress of the hydrogel decreased by about 32%, as shown in Fig. 3b. After the hydrogel was doped with different contents of MoO_{3-x} QDs, the 2% MoO_{3-x}-CDs-PVA hydrogel had the largest gel fraction and the lowest equilibrium swelling rate (Fig. 3c). Therefore, the 2% MoO_{3-x}-CDs-PVA hydrogel exhibits the best mechanical properties. The hydrogel with a self-healing ability can effectively improve the reliability and service life. Non-spontaneous repairable materials require additional

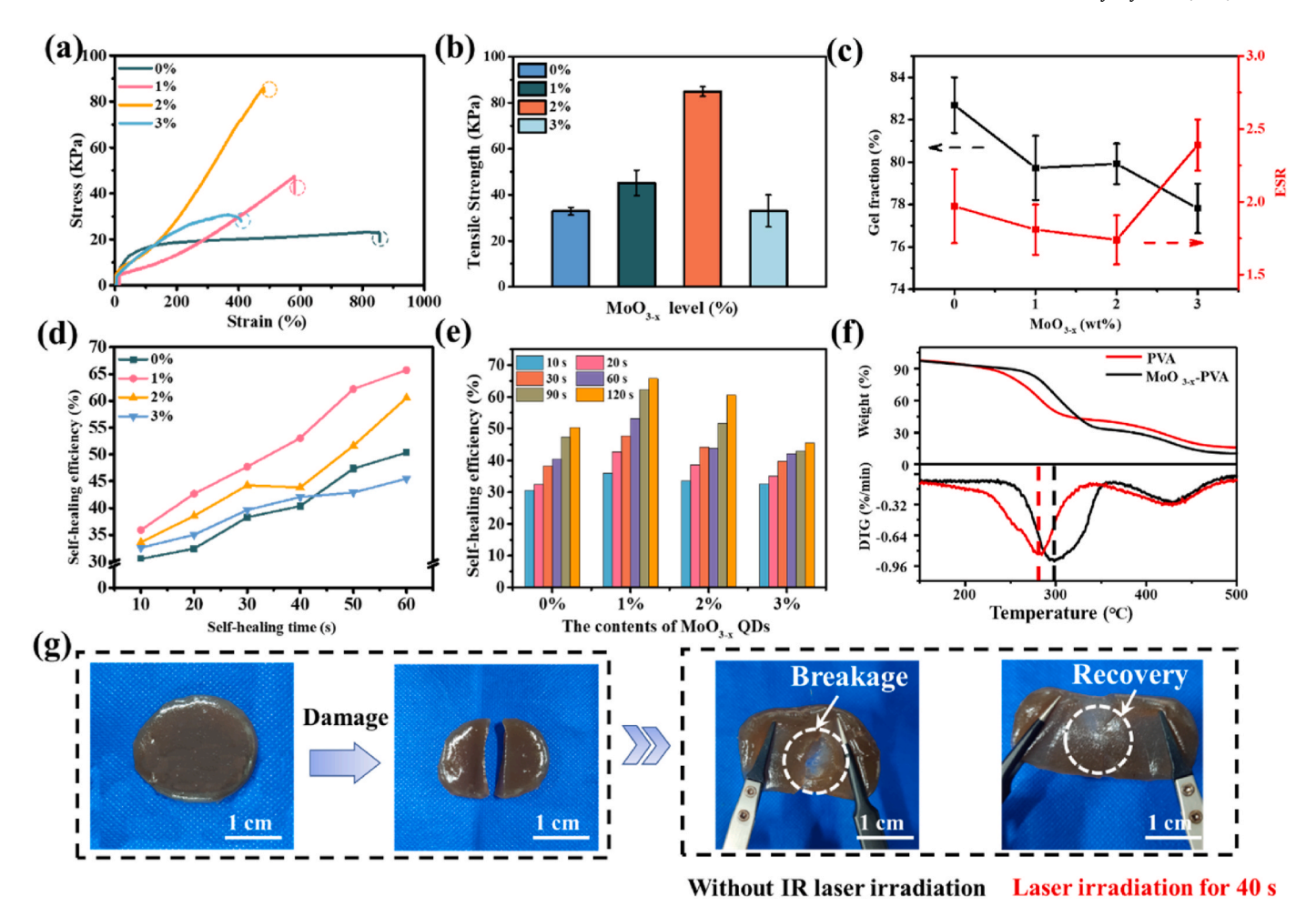


Fig. 3. (a) The tensile stress-strain curves of hydrogels with different MoO_{3-x} QDs contents. (b) Tensile strength of hydrogels with different MoO_{3-x} QDs contents. (c) The gel fraction and water equilibrium swelling ratio (ESR) of the PVA hydrogels with different MoO_{3-x} QDs loadings (d) Relationship between the self-healing efficiency and healing time of the hydrogel with different MoO_{3-x} QDs contents. (e) Healing efficiencies for hydrogels with different MoO_{3-x} QDs loadings under NIR irradiation. (f) TGA of the two samples under nitrogen atmosphere. (g) Photographs showing the self-healing process and behavior of the MoO_{3-x} -CDs-PVA hydrogel.

triggers or assistance to activate the repair process, but they still have many unique advantages in practical applications. We can precisely control the repair process of non-spontaneous repairable materials by adjusting the heating temperature or light intensity. These external stimuli can be used as switches to make the repair process of the materials controllable. The self-healing properties of the hydrogel were manifested by the self-healing efficiency which was defined as:

$$R = \delta_1/\delta_0 \times 100\% \tag{1}$$

where *R* represents the self-healing efficiency of the hydrogel, and δ_1 and δ_0 are the tensile stresses before and after the hydrogel underwent self-healing, respectively. The self-healing properties of the composite hydrogel with different MoO_{3-x} QDs are shown in Fig. 3d. The self-healing efficiency of different hydrogels increases with increasing healing time. However, as the content of MoO_{3-x} QDs is increased, the hydrogel gradually lost its self-healing properties (Fig. 3e). The stability of the hydrogel is characterized by the Thermogravimetric Experiment Analysis (TGA) (Fig. 3f). It is found that the MoO_{3-x}-CDs-PVA hydrogel exhibits thermal stability higher than that of the PVA hydrogel within a temperature range from 30 °C to 300 °C. Fig. 3g demonstrates the effect of infrared laser irradiation on the self-healing of the hydrogel. After being damaged, the composite hydrogel without infrared laser irradiation has poor self-healing performance compared with the one that is subjected to infrared laser irradiation. After self-healing, exerting the

same level of external loading can easily regenerate cracks at the damaged region for the samples without laser irradiation, while the ones with irradiation are intact.

3.4. The fluorescent properties of the composited hydrogel

The composite hydrogel exhibit photoluminescent properties stemming from the fluorescent quantum dots. The hydrogel is doped with a type of blue fluorescent quantum dot. The as-prepared manganese doped CDs were observed to be transparent under visible light and exhibited a bright blue luminescence when excited by 365 nm wavelength of light, as shown in Fig. S6. The photoluminescent characteristics of the synthesized B-CDs were investigated systematically using a fluorescent spectrometer at different wavelengths to analyze the emission properties. As shown in Fig. S7, the as-prepared B-CDs have the strongest emission, centered at 440 nm (\lambda em) when excited by a light source with a wavelength of 340 nm (λex). Subsequently, the fluorescent spectrum of the composite hydrogel revealed that the blue fluorescent effect of the B-CDs remained stable. In addition, after doping MoO_{3-x} QDs into the hydrogel, the fluorescent behavior is maintained under ultraviolet light (Fig. 4a). In previous works, we demonstrated for the first time that the hydrogel doped with photoluminescent quantum dots could be utilized for optical measurements [24]. However, due to the limitation of the properties of the hydrogels, the range is restricted and the sensitivity to small force is limited. As shown in Fig. 4b, the

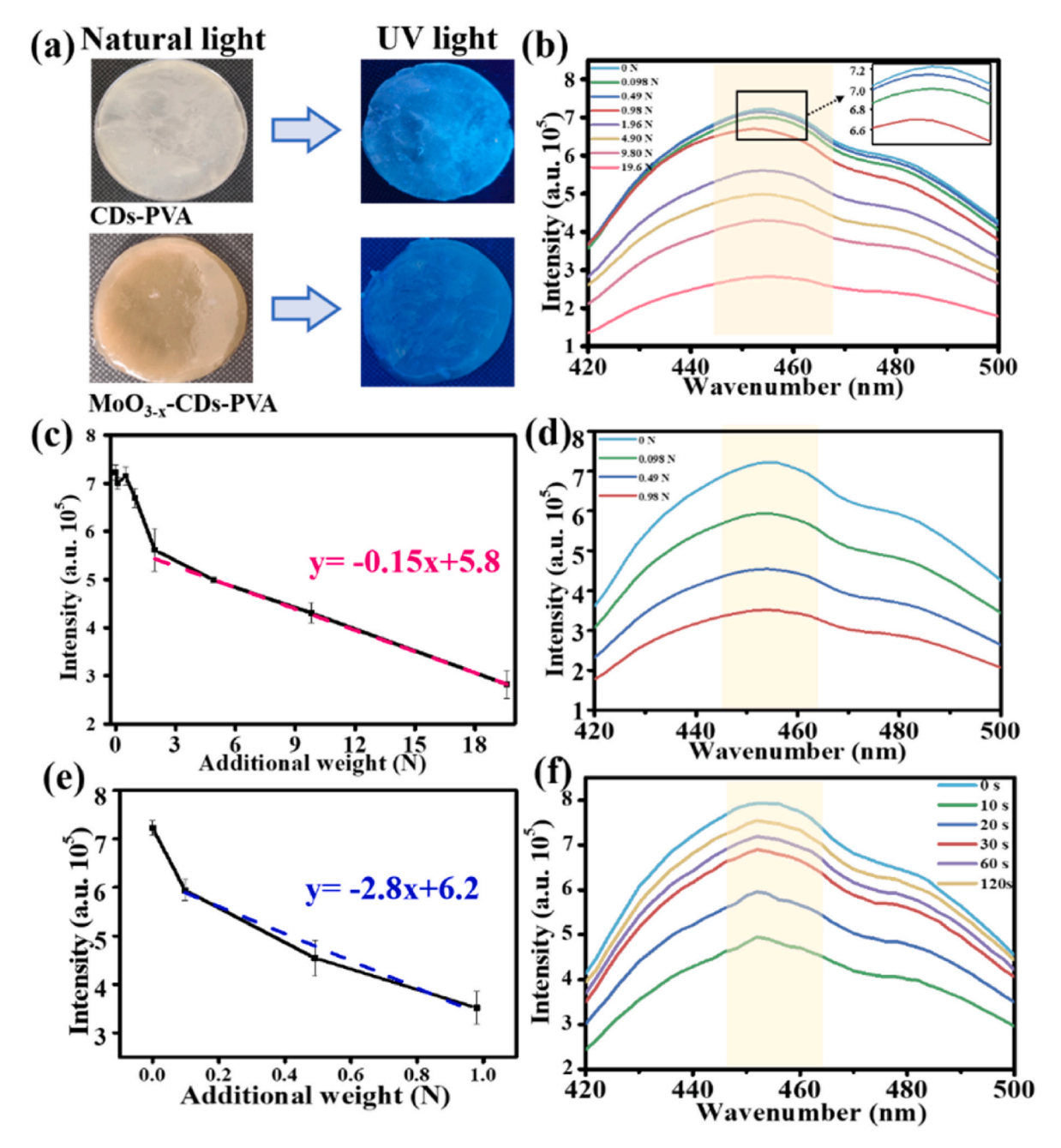


Fig. 4. (a) Photograph of CDs-PVA hydrogel and $MoO_{3.x}$ -CDs-PVA hydrogel under natural light and UV light. (b) Fluorescence spectra of hydrogel structure under different external forces. (c) A fitting curve of the fluorescence intensity of the hydrogel structure under different external forces. (d) Fluorescence spectrum of hydrogel under the action of small external force after infrared light irradiation. (e) A fitting curve of the fluorescence intensity of the hydrogel after infrared light irradiation. (f) Relationship between the fluorescence intensity of the hydrogel under different healing time.

fluorescence intensity of the hydrogels was tested under different external forces. When the external forces are larger than 0.98 N, there is a significant linear relationship between fluorescence intensity and the external force, indicating that the hydrogel has a good sensitivity within this force range (Fig. 4c). For less than 0.98 N of the force, the fluorescence intensity of the hydrogel is less sensitive. This motivates the incorporation of $\text{MoO}_{3\text{-x}}$ QDs in the hydrogel system. The sensitivity has scientifically improved for the molybdenum oxide-doped hydrogel with 30 s of infrared laser irradiation. Fig. 4d indicates that the optimal fluorescence emission wavelength of the composite hydrogel does not change after the hydrogel is irradiated by an infrared laser. However, the fluorescence intensity of the hydrogel changes more obviously after a small force is applied, and shows a good linear relationship, as shown in Fig. 4e. In addition, the self-healing capability of the hydrogel can be

determined by the fluorescence intensity. As the self-healing time increases, the healing effect improves, and its fluorescence intensity gradually increases. The fluorescence intensity of the damaged hydrogel positively correlates with the healing time, as shown in Fig. 4f.

3.5. Applications

Indirect mechanical monitoring of hydrogels can be applied in many fields. Fracturing is an important method for unconventional oil and gas production. And fracture feature analysis is one of the common methods to evaluate the effect of fracturing. The cracks at different locations in the rock extend along with the direction of the force. However, usually only the injection pressure can be obtained and the exact stress field and distribution are difficult to obtain in the process of fracturing. Therefore,

using a functional hydrogel as the medium helps to solve the problem. The changes in fluorescence intensity reflect the stress distribution of the core at various points during the fracturing process. The numerical value of the fluorescence intensity in the simulation field can be analyzed. As a result, the fracture trend after core fracturing can be predicted or estimated. The application of the MoO_{3-x}-CDs-PVA hydrogel on monitoring of core fracture is shown in Fig. 5a. The hydrogels are evenly distributed and attached at nine positions on the core before conducting the fluorescence intensity test. The test results are shown in Fig. 5b. The spectra show that the fluorescence intensity of the hydrogel at different positions has changed significantly. Fig. 5c is the pressure field diag plotted according to the fluorescence intensity. The simulated fracture pattern and the extended trend are consistent with the real fracture. At the same time, in the fields of petroleum exploration, hydrogeology, etc., accurately obtaining the pressure field distribution in porous media is also important for studying the fluid mechanics and transmission in it. Fig. 5d is a schematic diag of the distribution of the hydrogel in the porous media model, where the green mark represents the detection point of the hydrogel. As shown in Fig. 5e, the fluorescence intensity of the hydrogel at different points is inversely proportional to the pressure at that particular location. The pressure field distribution is obtained in the simulation by measuring the fluorescence intensity of the hydrogel as shown in Fig. 5f. The pressure field near the injection well is red, while the pressure field in the middle and the end of the model is blue, indicating the pressure variation in the model. The consumption is mainly concentrated near the injection well, and the displacement in the latter half of the model is relatively small, which is consistent with the report in the literature. The use of the current composite hydrogel can feasibly obtain the pressure distribution, avoiding the cumbersome process of using multiple sets of pressure sensors.

4. Discussion

In order to improve the healing efficiency and shorten the healing time of the hydrogel, we used an infrared laser to illuminate the hydrogel doped with photothermal MoO_{3-x} QDs. When the irradiation

time reached 40 s, the self-healing efficiency of the hydrogel reached the maximum value of 80%, as shown in Fig. 6a. The efficiency of selfhealing was doubled compared with that of no exposure to irradiation in the air. In addition, after 40 s of light irradiation (using 808 nm NIR laser), the healing efficiency of the hydrogel can reach to about 100% after another 20 s in the air without any external stimulus. The healing process of MoO_{3-x}-CDs-PVA hydrogel was activated by the temperature rise caused by the photothermal effect of MoO_{3-x} under NIR irradiation. In order to investigate the important role of higher thermal conductivity from MoO3-x QDs, another experiment was conducted, as shown in Fig. 6b. Both PVA and 2% MoO_{3-x}-CDs-PVA hydrogels were heated in an oven at 55 °C and their temperature changes were monitored. For the CDs-PVA hydrogel, the temperature increased to 50 °C within 7 min, while the 2% MoO_{3-x}-CDs-PVA hydrogel reached the same temperature in only 4 min, indicating that the 2% MoO_{3-x}-CDs-PVA hydrogel exhibited quick thermal responses. The thermal-sensitive physically crosslinked polymer chain become highly mobile, which can under diffusion, re-entangled to heal the damages. Therefore, the MoO_{3-x} QDs not only act as NIR photothermal conversion agents to transduce light into heat, but also transfer the heat into the hydrogel matrix quickly and homogenously. The healing process of the MoO_{3,v}-CDs-PVA hydrogel is depicted in Fig. 6c. First, the stable network structure of the hydrogel is damaged by applying an external force. As a result, the hydrogen bonds between the polymer chains, the polymer and the CDs, and the polymer and MoO_{3-x} QDs are ruptured in the damaged region. Then, under the NIR light, the well-dispersed MoO_{3-x} QDs transduce light into heat quickly. Then the PVA chain, the chitosan chain, and the agarose chain become mobile and the flexibility of the molecular chain also increases, facilitating the regeneration of the intermolecular hydrogen bonding. Finally, the network structure of the hydrogel is recovered upon removal of the light and cooling to room temperate. However, when the infrared irradiation is applied for a longer time, it causes the hydrogel to heat up too high, and the hydrogen bonds in the damaged part could not be reestablished due to the high temperature and high atomic motion, leading to permanent damage of the hydrogel. Therefore, proper irradiation intensity and time are the keys to achieving rapid and robust

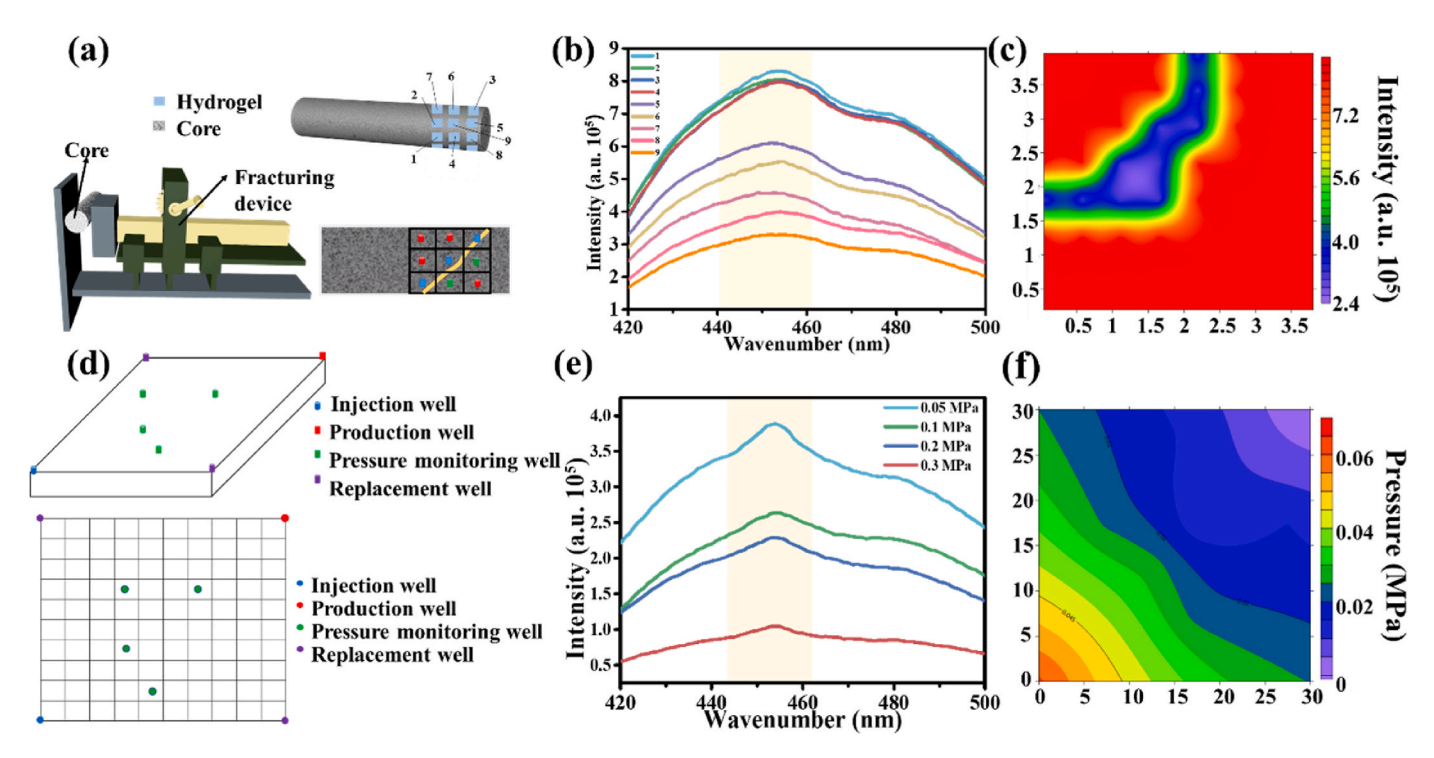


Fig. 5. (a) Schematic diag of the hydrogel used to detect the core fracturing fracture. (b) Fluorescent spectra of the hydrogel at different positions of core fractures. (c) Diag of pressure field distribution surrounding a fracture. (d) Schematic diag of fluid pressure distribution monitoring using the composite hydrogel. (e) Fluorescent spectra of the hydrogels in different parts of the fluid model. (f) Fluid distribution pressure field diag.

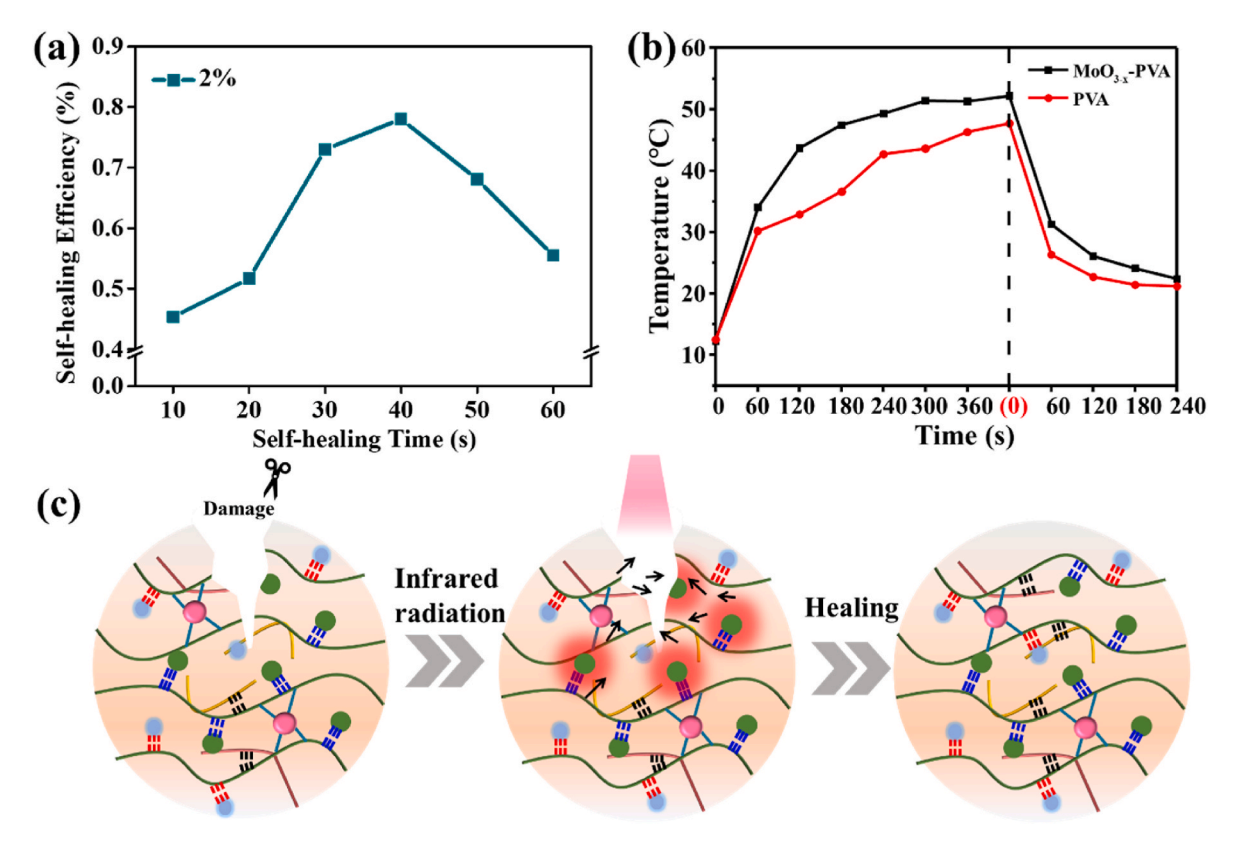


Fig. 6. (a) Self-healing efficiency of hydrogel with 2% MoO_{3-x} QDs for different irradiation duration. (b) Time-dependent temperature changes for PVA and MoO_{3-x}-CDs-PVA hydrogels at 55 °C. (c)The schematic illustration of the self-healing mechanism for MoO_{3-x}-CDs-PVA hydrogel under NIR light irradiation.

healing of the hydrogel. Introducing the MoO_{3-x} QDs to the MoO_{3-x} -CDs-PVA hydrogel provides a facile strategy for designing remotely-controllable self-healing materials.

As depicted in Fig. 7a, the fluorescent quantum dots are uniformly dispersed in the hydrogel rendering the photoluminescent properties. The different spacings of the B-CDs result in different intensities of fluorescence excitation, such that the external force could be measured

by measuring the fluorescence intensity [24]. The hydrogel in the mold will deform under a certain external force, thus the density of the B-CDs increases. The blocking effect between the B-CDs weakens the fluorescence of hydrogels. When an external force above a certain pressure limit is applied to the hydrogel, the composite hydrogel can detect the external mechanical loadings through the change of fluorescence intensity. However, when the external force fails to cause the minimum

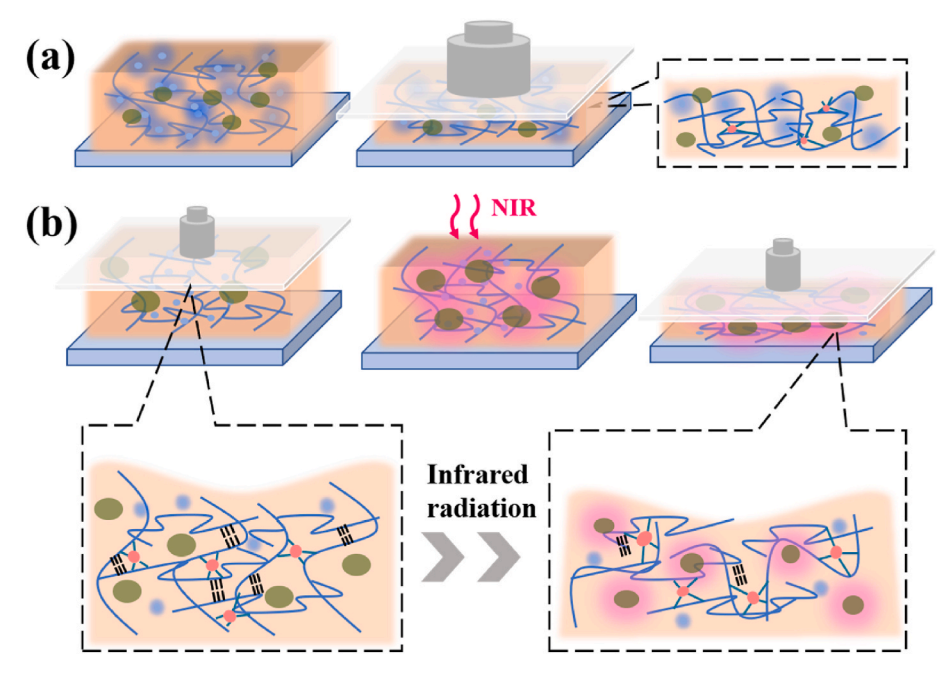


Fig. 7. (a) Schematic of the hydrogel structure under external forces. (b) Schematic diag of hydrogel structure under external force after infrared light irradiation.

level of the microscopic deformation of the hydrogel, the change in the fluorescence intensity of the hydrogel is not sufficient to reflect the influence of the external force. Introducing $\mathrm{MoO}_{3\text{-}x}$ QDs into the hydrogels helped to solve the problem of insensitivity to small external forces in the hydrogel force monitoring. The schematic diag of the detection mechanisms involving a small external force applied to the hydrogel is shown in Fig. 7b. When the hydrogel is irradiated by an infrared laser, the flexibility of the polymer chain increases and the hydrogen bonds between molecules disappear. A small force can deform the hydrogel and change the relative distance of the carbon dots in the hydrogel, thereby changing the fluorescence intensity.

5. Conclusions

We have fabricated a novel composite hydrogel material with photothermal and photoluminescent properties by introducing the MoO_{3-x} QDs and B-CDs into the PVA hydrogel. The maximum tensile strength of the hydrogel can reach 90 KPa and can improve its self-healing ability (by 50%) after 40 s of infrared laser irradiation. The composite hydrogel can monitor forces in the range of 0.98 N-19.6 N without external stimuli. The results show that after a threshold the fluorescence intensity and the external force maintain a good linear relationship. Infrared laser irradiation effectively enhances the photothermal effect and the monitoring range of hydrogel is improved for small forces below 0.98 N. It is demonstrated that this multifunctional hydrogel can be adopted in the field of petroleum engineering to determine the fracture trend and fluid model distribution during the fracturing process. The novel composite material may have a wide range of potential applications in various fields due to its excellent laser responsive characteristics, fluorescence characteristics, and force monitoring capabilities.

Author statement

Yiqiang Li: Conceptualization, Methodology, Provision, Formal analysis, Investigation, Writing e original draft Visualization, Yuanyuan Mi: Conceptualization, Formal analysis, Provision, Writing e original draft, Reviewing & Editing, Zheyu Liu: Visualization, Project administration, Funding acquisition, Supervision, Yinping Liu: Investigation, Formal analysis, Validation, Weiye Zhang: Formal analysis, Visualization, Shangxing Qiu: Investigation, Resources, Melvin A. Ramos: Writing e review & editing, Supervision, Travis Shihao Hu: Methodology, Quan Xu: Writing e review & editing, Supervision, Funding acquisition.

Declaration of competing interest

The authors declare that they have no known competing financial interests or personal relationships that could have appeared to influence the work reported in this paper.

Data availability

Data will be made available on request.

Acknowledgments

This work was supported by the National Natural Science Foundation of China (No. 51875577), National Key Research and Development Plan (No. 2020YFC1808102), Science Foundation of China University of Petroleum (No. 2462020YXZZ018, 2462019QNXZ02, 2462022BJRC005) and the U.S. National Science Foundation (Award No. 2004251).

Appendix A. Supplementary data

Supplementary data to this article can be found online at https://doi.org/10.1016/j.mtphys.2022.100807.

References

- [1] S.L. Banerjee, K. Bhattacharya, S. Samanta, N.K. Singha, Self-healable antifouling zwitterionic hydrogel based on synergistic phototriggered dynamic disulfide metathesis reaction and ionic interaction, ACS Appl. Mater. Interfaces 10 (32) (2018) 27391–27406, https://doi.org/10.1021/acsami.8b10446.
- [2] M. Wang, Y. Chen, R. Khan, H. Liu, C. Chen, T. Chen, R. Zhang, H. Li, A fast self-healing and conductive nanocomposite hydrogel as soft strain sensor, Colloid Surf. A-Physicochem. Eng. Asp. 567 (2019) 139–149, https://doi.org/10.1016/j.colsurfa.2019.01.034.
- [3] Y. Amamoto, H. Otsuka, A. Takahara, K. Matyjaszewski, Self-healing of covalently cross-linked polymers by reshuffling thiuram disulfide moieties in air under visible light, Adv. Mater. 24 (29) (2012) 3975–3980, https://doi.org/10.1002/ adma.201201928.
- [4] Y. Guan, Y. Zhang, Boronic acid-containing hydrogels: synthesis and their applications, Chem. Soc. Rev. 42 (20) (2013) 8106–8121, https://doi.org/ 10.1039/C3CS60152H.
- [5] D. Zhu, Q. Ye, X. Lu, Q. Lu, Self-healing polymers with PEG oligomer side chains based on multiple H-bonding and adhesion properties, Polym. Chem. 6 (28) (2015) 5086–5092, https://doi.org/10.1039/C5PY00621J.
- [6] M. Wei, Y. Zhang, D. Yu, H. Xie, M. He, K. Yang, Y. Wang, Novel poly (tetramethylene ether)glycol and poly(ε-caprolactone) based dynamic network via quadruple hydrogen bonding with triple-shape effect and self-healing capacity, ACS Appl. Mater. Interfaces 7 (4) (2015) 2585–2596, https://doi.org/10.1021/ am507575x
- [7] L. Shi, P. Ding, Y. Wang, Y. Zhang, D. Ossipov, J. Hilborn, Self-healing polymeric hydrogel formed by metal-ligand coordination assembly: design, fabrication, and biomedical applications, Macromol. Rapid Commun. 40 (7) (2019): 1800837, https://doi.org/10.1002/marc.201800837.
- [8] Q. Zhang, X. Zhu, C.-H. Li, Y. Cai, X. Jia, Z. Bao, Disassociation and reformation under strain in polymer with dynamic metal–ligand coordination cross-linking, Macromolecules 52 (2) (2019) 660–668, https://doi.org/10.1021/acs. macromol.8b02414.
- [9] J.H. KIm, S.W. Kim, J. Kim, D.-Y. Chung, T.-H. Kim, K.H. Jo, J.H. Hahn, Z. Bao, S. Hwang, N. Park, Polypyrrole/agarose-based electronically conductive and reversibly restorable hydrogel, ACS Nano 8 (10) (2014) 10066–10076, https://doi. org/10.1021/nn502704g.
- [10] Y. Shi, M. Wang, C. Ma, Y. Wang, X. Li, G. Yu, A conductive self-healing hybrid gel enabled by metal-ligand supramolecule and nanostructured conductive polymer, Nano Lett. 15 (9) (2015) 6276–6281, https://doi.org/10.1021/acs. nanolett.5b03069.
- [11] C. Ghobril, K. Charoen, E.K. Rodriguez, A. Nazarian, M.W. Grinstaff, A dendritic thioester hydrogel based on thiol-thioester exchange as a dissolvable sealant system for wound closure, Angew. Chem.-Int. Edit. 52 (52) (2013) 14070–14074, https://doi.org/10.1002/anie.201308007.
- [12] C. Yu, C.F. Wang, S. Chen, Robust self-healing host-guest gels from magnetocaloric radical polymerization, Adv. Funct. Mater. 24 (9) (2014) 1235–1242, https://doi. org/10.1002/adfm.201302058.
- [13] Y. Li, G. Huang, X. Zhang, B. Li, Y. Chen, T. Lu, T.J. Lu, F. Xu, Magnetic hydrogels and their potential biomedical applications, Adv. Funct. Mater. 23 (6) (2013) 660–672, https://doi.org/10.1002/adfm.201201708.
- [14] Y. Zhang, B. Yang, X. Zhang, L. Xu, L. Tao, S. Li, Y. Wei, A magnetic self-healing hydrogel, Chem. Commun. 48 (74) (2012) 9305–9307, https://doi.org/10.1039/ C2CC34745H
- [15] E. Zhang, T. Wang, L. Zhao, W. Sun, X. Liu, Z. Tong, Fast self-healing of graphene oxide-hectorite clay-poly(N,N-dimethylacrylamide) hybrid hydrogels realized by near-infrared irradiation, ACS Appl. Mater. Interfaces 6 (24) (2014) 22855–22861, https://doi.org/10.1021/am507100m.
- [16] K. Haraguchi, K. Uyama, H. Tanimoto, Self-healing in nanocomposite hydrogels, Macromol. Rapid Commun. 32 (16) (2011) 1253–1258, https://doi.org/10.1002/marc.201100248.
- [17] M. Park, J. Park, U. Jeong, Design of conductive composite elastomers for stretchable electronics, Nano Today 9 (2) (2014) 244–260, https://doi.org/ 10.1016/j.nantod.2014.04.009.
- [18] S. Li, C. Gao, X. Xu, X. Bai, H. Wang, N. Gao, C. Feng, Y. Xiong, M. Liu, Injectable and self-healing carbohydrate-based hydrogel for cell encapsulation, ACS Appl. Mater. Interfaces 7 (23) (2015) 13029–13037, https://doi.org/10.1021/ acsami.5b00389.
- [19] A. Phadke, C. Zhang, B. Arman, C.C. Hsu, R.A. Mashelkar, A.K. Lele, M.J. Tauber, G. Arya, S. Varghese, Rapid self-healing hydrogels, Proc. Natl. Acad. Sci. USA 109 (12) (2012) 4383, https://doi.org/10.1039/D0QM01099E.
- [20] Z. Wei, J. He, T. Liang, H. Oh, J. Athas, Z. Tong, C. Wang, Z. Nie, Autonomous self-healing of poly(acrylic acid) hydrogels induced by the migration of ferric ions, Polym. Chem. 4 (17) (2013) 4601–4605, https://doi.org/10.1039/C3PY00692A.
- [21] J. Canadell, H. Goossens, B. Klumperman, Self-healing materials based on disulfide links, Macromolecules 44 (8) (2011) 2536–2541, https://doi.org/10.1021/ ma2001402
- [22] H. Li, Y. Li, Q. Xu, A. Zhang, Multifunctional clay/PNIPAM hydrogel incorporating HxMoO₃ plasmonic quantum dot, Energy Environ. Mater. 3 (2) (2020) 192–201, https://doi.org/10.1002/eem2.12066.
- [23] W. Xu, W. Wang, S. Chen, R. Zhang, Y. Wang, Q. Zhang, L. Yuwen, W.J. Yang, L. Wang, Molybdenum disulfide (MoS₂) nanosheets-based hydrogels with lighttriggered self-healing property for flexible sensors, J. Colloid Interface Sci. 586 (2021) 601-612, https://doi.org/10.1016/j.jcis.2020.10.128.
- [24] M. Li, W. Li, W. Cai, X. Zhang, Z. Wang, J. Street, W.-J. Ong, Z. Xia, Q. Xu, A self-healing hydrogel with pressure sensitive photoluminescence for remote force

- measurement and healing assessment, Mater. Horiz. 6 (4) (2019) 703–710, https://doi.org/10.1039/C8MH01441H.
- [25] Q. Yan, W. Xie, M. Zhou, H. Fu, An ultrasensitive and highly compressive piezoresistive sensor based on a biopolyol-reinforced polyurethane sponge coated with silver quantum dotss and carbon nanotubes/cellulose nanocrystals, J. Mater. Chem. C 8 (46) (2020) 16603–16614, https://doi.org/10.1039/D0TC04141F.
- [26] Y. Tan, K. Ivanov, Z. Mei, H. Li, L. Lubich, H. Li, C. Wang, L. Wang, A soft wearable and full textile piezoresistive sensor for plantar pressure capturing, Micromachines 12 (2) (2021) 110, https://doi.org/10.3390/mi12020110.
- [27] Y. Chen, C. Hu, Z. Wang, Y. Li, S. Zhu, W. Su, Z. Hu, Z. Zhou, M. Liu, Wireless strain sensor based on the magnetic strain anisotropy dependent ferromagnetic resonance, AIP Adv. 10 (10) (2020): 105310, https://doi.org/10.1063/5.0022900.
- [28] D. Ding, W. Guo, C. Guo, J. Sun, N. Zheng, F. Wang, M. Yan, S. Liu, MoO_{3-x} quantum dots for photoacoustic imaging guided photothermal/photodynamic cancer treatment, Nanoscale 9 (5) (2017) 2020–2029, https://doi.org/10.1039/ CCND000461.
- [29] L. He, D. Szopinski, Y. Wu, G.A. Luinstra, P. Theato, Toward self-healing hydrogels using one-pot thiol-ene click and borax-diol chemistry, ACS Macro Lett. 4 (7) (2015) 673–678, https://doi.org/10.1021/acsmacrolett.5b00336.
- [30] T. Liu, X. Peng, Y.-N. Chen, Q.-W. Bai, C. Shang, L. Zhang, H. Wang, Hydrogen-bonded polymer-small molecule complexes with tunable mechanical properties, Macromol. Rapid Commun. 39 (2018): 1800050, https://doi.org/10.1002/marc.201800050.